mathematics

Article

Oscillatory and Periodical Behavior of Heat Transfer and Magnetic Flux along Magnetic-Driven Cylinder with Viscous Dissipation and Joule Heating Effects

Zia Ullah [1,*], Musaad S. Aldhabani [2] and Muhammad Adnan Qaiser [3]

[1] Department of Mathematics and Statistics, The University of Lahore, Sargodha-Campus, Sargodha 40100, Pakistan
[2] Department of Mathematics, Faculty of Science, University of Tabuk, P.O. Box 741, Tabuk 71491, Saudi Arabia; maldhabani@ut.edu.sa
[3] College of Physics and Optoelectronic Engineering, Shenzhen University, Shenzhen 518060, China; muhammad.adnan.vt0591@iiu.edu.pk
* Correspondence: ziakhan.uos.72@gmail.com or ziaullah.khan@math.uol.edu.pk

Abstract: Several primary mechanisms are less utilized in engineering and recent technologies due to unsustainable heating. The impact of viscous dissipation and Joule heating is very important to examine current density and heat rate across a magnetized cylinder. The key objective of this examination was to insulate excessive heat around the cylinder. The present effort investigated the impact of viscous dissipations, Joule heating, and magnetohydrodynamics (MHD) on the transitory motion of convective-heat transport and magnetic flux features of dissipative flows throughout a magnetized and warmed cylinder at suitable places. The suggested turbulent dynamical structure of mathematics is offered for an associated method of partial differentiation equations impacted by boundary values. The complex equations are translated via non-dimensional shapes by using relevant non-dimensional numbers. The non-dimensional representation has been improved to make it easier to conduct uniform computational calculations. The computational answers for these linked dimensionalized formulations have been achieved using the Prandtl coefficient Pr, Joule heating parameter ζ, Eckert number E_c, the magneto-force number ξ, the buoyancy parameter λ, and multiple additional predefined factors. The important contribution of this work is based on non-fluctuating solutions that are utilized to examine the oscillating behavior of shearing stress, rate of fluctuating heat transport, and rate of fluctuating magnetic flux in the presence of viscous dissipation and Joule heating at prominent angles. It is shown that the velocity of a fluid increases as the buoyancy parameter increases. The maximum frequency of heat transmission is illustrated for each Eckert variable.

Keywords: viscous dissipation; Joule heating; periodic flow; oscillations; heat transfer; magnetic flux; heated cylinder

MSC: 80M20

check for updates

Citation: Ullah, Z.; Aldhabani, M.S.; Qaiser, M.A. Oscillatory and Periodical Behavior of Heat Transfer and Magnetic Flux along Magnetic-Driven Cylinder with Viscous Dissipation and Joule Heating Effects. *Mathematics* **2023**, *11*, 3917. https://doi.org/10.3390/math11183917

Academic Editor: Yang Liu

Received: 9 August 2023
Revised: 4 September 2023
Accepted: 12 September 2023
Published: 14 September 2023

1. Introduction

Considering the widespread use of numerous manufacturing and mechanical applications, from thermal exchanger chambers, ventilation heaps, cooling structures, assessment instruments, detectors, the transpiration of different substances (textiles, veneers, papers, and film ingredients), cooled transparent materials, polymers, mechanical parts, and blades of turbines to electrical systems, anemometry, and organic or radiated contamination/purification, the flow of heat about a cylindrical object has been the target of analysis. It occurs exclusively by natural convection or forced convection in particular procedures. However, there are other systems in which both forced and natural convection are of equivalent orders with the mechanism of heat transfer referred to mixed convection. Viscous dissipation is used as the source of energy, transforming temperature gradients and consequently improving heat exchange levels. The significance of dissipation from viscous material varies depending on whether the cylinder is warm or cold. Poornima et al. [1] provided a computational framework to represent an intensely opaque liquid passing through an insulating rotating cylinder that is hosting a chemical function. The outermost part of the cylinder was exposed to a transversal fixed and consistent electromagnetic field. Considering the nonlinear tiny fluids under thermal boundary parameters, Mahat et al. [2] examined computationally the effect of dissipations on sustained two-dimensional combined convection flow across a straight round cylinder. Mohamed et al. [3] performed the numerical simulation of convection–conduction flow separation across a plain round cylinder using a tiny liquid based on the dissipating viscous action. Anwar et al. [4] examined graphically the continuous convection-driven flow separation of a dynamic liquid across a straight round cylinder in a channel moving upwards in both the warmed and coolant cylinder situations. Aboud et al. [5] used the Galerkin approach with finite elements to computationally explore the aqueous movement and convection-driven heat transmission of a non-Newtonian nanofluid-filled round annular cylinder enclosed in a field of magnets for a steady-state, impermeable, laminar stream. The influence of magnetohydrodynamics on the velocity of an electrically conducting fluid in magnetic regions was investigated in [6]. Due to its uses in the construction of heat exchangers and nuclear reactors, the phenomenon has considerable potential. Makanda et al. [7] examined the influence of radioactivity on MHD conduction from a cylindrical structure containing significant slip in a Casson solution with non-Darcy transparent medium. Gireesha et al. [8] investigated the implications of mixed thermal motion of non-Newtonian fluids induced by a stretchy surface that is naturally warmed with small particles of dust.

In production and manufacturing technologies, the consequences of viscous dissipation for the movement of heat is an essential subject. The implications of the magnetic hydrodynamics for oscillating thermal and magneto-fluid motion have received essential consideration in heated up/metal extraction, micro devices for electronics, geography, and metalworking disciplines. Employing the above-mentioned MHD and thermal transfer concepts, several academics have investigated natural or forced convection thermal transfer procedures in both nonmagnetic and ionized geometries, such as vertically warmed plates, elliptical cylinders, ionized spheres, plumes, and nano permeable tubes. In [9], the researcher assessed the implications of the enclosed surface with nanoparticles for the natural heat process. Entropy assessment of circular pseudoplastic movement with hydromagnetic input by employing the Keller box methodology was carried out computationally in [10]. Zhang et al. [11] explored a situation where two analogous consecutive concentric cylinders were contained in a duct and subjected to an ambient transverse magnetic attraction. The effects of the magnetic attraction, the motion of the conductive flow at the intake, the separation rate on fluid movement systems, the periodicity of shedding vortex, pressure gradient variables, drag factors, and the variation in pressure were explored. By using a power series expansion, Naghshineh et al. [12] investigated the statistical results for the flow-separation mechanism for Ostwald-de Waele power law materials. Khan et al. [13] addressed the impacts of magnetohydrodynamics, permeable media, and mixed convection on the stationary region movement of non-Newtonian fluids. In [14], the investigator derived the mathematical models of an unstable two-dimensional incompressible viscous electrically charged hydrogel under an applied electromagnetic field through the theory of distributed-order Maxwell and Cattaneo parametric connections. The Marangoni transformed thermal motion of the Casson material through a vertically stratified channel was described by Hayat et al. [15]. By using a consistent magnetic field, the author [16] investigated the Stokesian movement of an axisymmetric, inflexible pair-stressed fluid over an impermeable substance surrounding an opaque sphere. Routa et al. [17] investigated how fluid movement and thermal transport mechanisms along a cylinder were impacted by ground topography, dynamic behavior, and rotational motion. Incorporating the power-law modeling for hydrodynamic behavior, the sinusoidal topographic model was used to influence the roughness features. Applying computer modeling, Junbo and Yongming [18] focused on the naturally occurring movement of water boundary layers on heated/cooled smooth plates. It was investigated how the phase change was affected by the wall temperature, incoming stream speed, and incoming stream heating. The properties of double-diffusive combined convective motion in the upward channel with viscous stratification's continuous instability were studied by Ankush [19]. The effects of dissipations, solar radiations, and Ohmic energy on the magnetohydrodynamic pulsating motion of a third-grade hybrid nanofluid in an impermeable surface were studied in [20]. The influence of the outflow boundary variables on the consistency of insoluble fluids in a region containing permeable boundaries was researched by IIin and Morgulis [21].

The researchers utilized several kinds of strategies, namely the series approach, Karman Pohlhausen modeling, the finite-element strategy, and the firing approach, to arrive at computational findings for particular boundary requirements. A variety of surface-based, aircraft-based and space-based evaluation centers make it feasible in MHD and heat-generating conditions. The consequence of a heating source or sinking on the frequency of periodic convective motion through electrically conductive cylinders has not yet been evaluated. Utilizing the ideas of oscillation movement, heat exchange, magnetohydrodynamics, and thermal sources, a mathematical framework for the present phenomenon in nature has been created. Considering radiation, a nonuniform heat source, and a porous material, Kumar [22] addressed the Joule energy implication and chemical change on an unstable hydromagnetic free convective micropolar fluid across a stretched surface. To explore the Joule heating effect on mixed-convection MHD dissipative and radiative movement of an immiscible Jeffrey fluid caused by a stretched surface with power law thermal gradient, heat source/sink, and suction, Kumar [23] designed a mathematical model. To ensure the study's precision and validity, the authors estimated the friction factor, heat transfer rates, and mass transfer rates under certain confirmed conditions. The results were then compared to prior literature. A micropolar fluid's MHD free/forced convective flow past a wedge set in a variable-free stream and surface temperature was studied by Roy et al. [24]. They observed that the amplitudes of skin friction and couple stress increased with the increase in the Richardsons number. Fluctuating laminar free/forced convective fluid flow along a vertical wedge caused by oscillations in the free stream and surface temperature was discussed by Roy and Hossain [25]. Firoza et al. [26] analyzed combined mass-heat transmission over an oscillating free/forced convective flow across the vertical wedge with inclusion of radiation. Fluctuating free/forced convective dusty fluid flow via a vertical wedge caused by a minor variation in the free stream and surface temperature was examined by Hossain et al. [27]. The mass absorption problems with magnetohydrodynamic and radiation influences on viscous fluid through a stretching structure were researched by Maranna et al. [28]. Mabood et al. [29] successfully conducted Jeffrey tiny fluid systems with enthalpy and MHD implications within a flexible shape using a variety of technological solutions. The magnetic flux characteristics around the vertical and circular geometries were investigated in [30–34]. The comparison of results has been illustrated by Chawla [35]. The dual-temperature condensing and dual-temperature evaporating approach has been offered for the higher-temperature heat-pump system by incorporating the methodologies of ejection and two-phase compressors in order to attain the objective of neutralizing carbon for usage of heating in factories to recovering wasted energy in [36]. A trans-critical CO2 heating and ventilation engine with specific hydraulic sub-cooling was tested using a simulation for sustainability and socioeconomic evaluation in [37].

The significant novelty of the present research is to elaborate the oscillatory and periodical behavior of heat transfer and magnetic flux across various angles of a magnetized cylinder. For heat, mass and flow behavior, the continuity, momentum, energy and mass equations were derived in the form of partial differential equations. The governing equations were transformed into unit-less form by using dimensionless variables. The current problem is very important for insulating material to decrease excessive heating. This is a well-numerated effort for the physical mechanism using a finite difference scheme and Gaussian elimination technique. Due to excessive heating, various mechanisms are less interesting in engineering and industrial processes. To overcome this issue in current analysis, the surface is magnetized, and the fluid is electrically conducting, which is responsible for reducing excessive heating along the surface. It is pertinent to mention here that the convective heat transfer is practically associated with oscillatory flow behavior. In the literature, various unsteady models are converted into ordinary equations and just solved for the steady part, but in the current work, the periodic behavior of skin friction, heat transfer and magnetic flux is obtained by using oscillating Stokes conditions. The results are excellent and accurate because they are satisfied by the given boundary conditions. Based on the findings of the research overview, the oscillating hybrid thermal motion of oscillating energy and oscillating magnetic flux through a magnetized warmed cylinder has not been explored in terms of dissipations and Joule heating. The periodical and fluctuating hybrid convection magneto-thermo movement inside the magnetic cylinder at notable points was initially created via principles of preceding research and the findings of [3,7,13]. The periodic heat transport, fluctuating friction coefficients, and oscillatory magnetic flux values are illustrated by using velocity distributions, magnetic distributions, and temperature distributions at prominent angles. The main novelty of the current work is to compute the amplitude of fluctuating heat transfer and oscillatory magnetic flux along a magnetized heated cylinder.

2. Flow Formulation

Consider the laminar, time-dependent fluctuating mixed convective boundary layer movement mechanism across a horizontal, heating geometry at sharp angles $\pi/3$ and π. Figure 1 shows coordinate axes of cylindrical geometry with x and y directions. The components u and v describe the x- and y-directional velocity elements, correspondingly. The term H_y is the factor of normal electromagnetic region, and H_x depicts the element of electric field at the outer boundary of the cylindrical shape; the wall temperature of the cylindrical shape is T_w, T_∞ is ambient temperature of cylindrical diagram, H_o is minimum magnetic magnitude exact at the horizontal heating geometry. Additionally, the gravity force is acting downward. The boundary layer equation's dimensioned form shows the flow behavior as

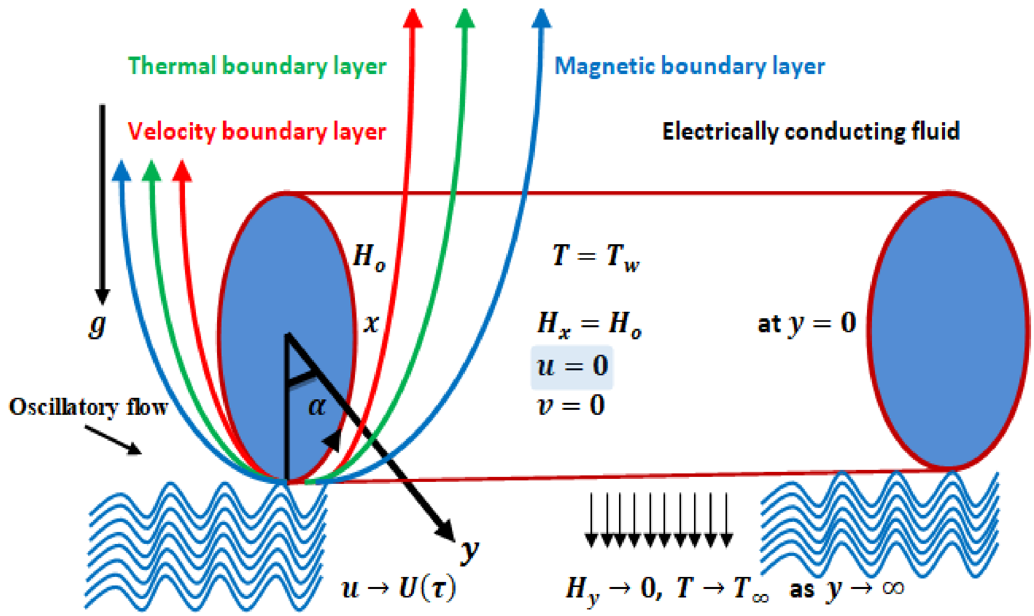

Figure 1. Magnetized heated cylinder and coordinate system.

$$\frac{\partial \overline{u}}{\partial \overline{x}} + \frac{\partial \overline{v}}{\partial \overline{y}} = 0 \tag{1}$$

$$\frac{\partial \overline{u}}{\partial \tau} + \overline{u}\frac{\partial \overline{u}}{\partial \overline{x}} + \overline{v}\frac{\partial \overline{u}}{\partial \overline{y}} = \frac{\mathrm{d}\overline{\mathrm{U}}}{\mathrm{d}\tau} + \frac{\partial^2 \overline{u}}{\partial \overline{y}^2} + \xi\left(\overline{h}_x \frac{\partial \overline{\mathrm{h}}_{\mathrm{x}}}{\partial \overline{y}} + \overline{h}_y \frac{\partial \overline{\mathrm{h}}_{\mathrm{x}}}{\partial \overline{y}}\right) + \lambda\theta sin\alpha \tag{2}$$

$$\frac{\partial \overline{\mathrm{h}}_{\mathrm{x}}}{\partial \overline{x}} + \frac{\partial \overline{\mathrm{h}}_{\mathrm{y}}}{\partial \overline{y}} = 0 \tag{3}$$

$$\frac{\partial \overline{\mathrm{h}}_x}{\partial \tau} + \overline{u}\frac{\partial \overline{\mathrm{h}}_x}{\partial \overline{x}} + \overline{v}\frac{\partial \overline{\mathrm{h}}_x}{\partial \overline{y}} - \overline{h}_x\frac{\partial \overline{\mathrm{u}}}{\partial \overline{x}} - \overline{h}_y\frac{\partial \overline{\mathrm{u}}}{\partial \overline{y}} = \frac{1}{\gamma}\frac{\partial^2 \overline{\mathrm{h}}_x}{\partial \overline{y}^2} \tag{4}$$

$$\frac{\partial \overline{\theta}}{\partial \tau} + \overline{u}\frac{\partial \overline{\theta}}{\partial \overline{x}} + \overline{v}\frac{\partial \overline{\theta}}{\partial \overline{y}} = \frac{1}{P_r}\frac{\partial^2 \overline{\theta}}{\partial \overline{y}^2} + \zeta\overline{u}^2 + E_c\left(\frac{\partial \overline{u}}{\partial \overline{y}}\right)^2 \tag{5}$$

Non-dimensional boundary values are:

$$\overline{u}(0) = 0,\ \overline{v}(0) = 0,\ \overline{\theta}(0) = 1,\ \overline{h}_y(0) = 0,\ \overline{h}_x(0) = 1 \text{ at } \overline{y} = 0, \tag{6}$$

$$\overline{u}(\infty) \to \overline{U}(\tau),\ \overline{\theta}(\infty) \to 0,\ \overline{h}_x(\infty) \to 0\,,\ \text{as } \overline{y} \to \infty.$$

In the above Equations (1)–(5), using proposed boundary conditions (6), mixed convective parameters λ and ζ represent the variable surface temperature number, γ is the magnetic Prandtl parameter, Pr stands for Prandtl parameter, ξ represents the electromagnetic force number, Eckert number, and Joule heat factor and is defined in Equation (7).

$$\begin{gathered} \alpha = \tfrac{\kappa}{\rho C_p},\ \lambda = \tfrac{G_{r_L}}{{Re_L}^2},\ Re_L = \tfrac{U_\infty L}{\nu},\ \theta = \tfrac{\overline{T}-\overline{T}_\infty}{\overline{T}_w-\overline{T}_\infty},\ P_r = \tfrac{\nu}{\alpha},\ G_{r_L} = \tfrac{g\beta\Delta T L^3}{\nu^2},\ \gamma = \tfrac{\nu}{\nu_m}, \\ \xi = \tfrac{\mu {H_0}^2}{\rho {U_\infty}^2},\ \zeta = \tfrac{\sigma L {B_o}^2 U_\infty}{\rho C_p \Delta T},\ E_c = \tfrac{{U_\infty}^2}{C_p\Delta T} \end{gathered} \tag{7}$$

The coupled nonlinear equations are converted into steady and unsteady parts by using oscillatory Stokes conditions given in Equation (8) by following [30–34].

$$\begin{gathered} \overline{u} = u_0 + \epsilon u_t e^{i\omega\tau},\ \overline{v} = v_0 + \epsilon v_t e^{i\omega\tau},\ \overline{h}_x = \mathrm{h}_{xo} + \epsilon \mathrm{h}_{xt} e^{i\omega\tau},\ \overline{h}_y = \mathrm{h}_{yo} + \epsilon \mathrm{h}_{yt} e^{i\omega\tau}, \\ \overline{\theta} = \theta_0 + \epsilon\theta_{\mathrm{t}} e^{i\omega\tau},\ \overline{U}(\ \tau\ ) = 1 + \epsilon e^{i\omega\tau},\ |\varepsilon| << 1 \end{gathered} \tag{8}$$

For steady components:

$$\frac{\partial u_0}{\partial x} + \frac{\partial v_0}{\partial y} = 0 \tag{9}$$

$$u_0\frac{\partial u_0}{\partial x} + v_0\frac{\partial u_0}{\partial y} = \frac{\partial^2 u_0}{\partial y^2} + \xi\left(h_{xo}\frac{\partial h_{xo}}{\partial x} + h_{yo}\frac{\partial h_{xo}}{\partial y}\right) + \lambda\theta_o sin\alpha \tag{10}$$

$$\frac{\partial h_{xo}}{\partial x} + \frac{\partial h_{yo}}{\partial y} = 0 \tag{11}$$

$$u_o\frac{\partial h_{xo}}{\partial x} + v_o\frac{\partial h_{xo}}{\partial y} - h_{xo}\frac{\partial u_o}{\partial x} - h_{yo}\frac{\partial u_o}{\partial y} = \frac{1}{\gamma}\frac{\partial^2 h_{xo}}{\partial y^2} \tag{12}$$

$$u_o\frac{\partial \theta_o}{\partial x} + v_o\frac{\partial \theta_o}{\partial y} = \frac{1}{P_r}\frac{\partial^2 \theta_o}{\partial y^2} + \zeta {u_o}^2 + E_c\left(\frac{\partial u_o}{\partial y}\right)^2 \tag{13}$$

with appropriate boundary conditions:

$$u_0 = 0,\ v_0 = 0,\ \theta_0 = 1,\ \mathrm{h}_{y0} = 0,\ \mathrm{h}_{x0} = 1 \text{ at } y = 0, \tag{14}$$

$$u_0 \to 1,\ \theta_0 \to 1,\ \mathrm{h}_{x0} \to 1\ ,\ \text{as } y \to \infty.$$

For unsteady components:

$$\frac{\partial u_t}{\partial x} + \frac{\partial v_t}{\partial y} = 0 \tag{15}$$

$$\begin{aligned} i\omega(u_t - 1) \quad & + u_o \tfrac{\partial u_t}{\partial x} + u_t \tfrac{\partial u_o}{\partial x} + v_o \tfrac{\partial u_t}{\partial y} + v_t \tfrac{\partial u_o}{\partial y} \\ & = \tfrac{\partial^2 u_t}{\partial y^2} + \xi\left(h_{xo}\tfrac{\partial h_{xt}}{\partial x} + h_{xt}\tfrac{\partial h_{xo}}{\partial x} + h_{yo}\tfrac{\partial h_{xt}}{\partial y} + h_{yt}\tfrac{\partial h_{xo}}{\partial y}\right) + \lambda \theta_t sin\alpha \end{aligned} \tag{16}$$

$$\frac{\partial h_{xt}}{\partial x} + \frac{\partial h_{yt}}{\partial y} = 0 \tag{17}$$

$$\begin{aligned} i\omega h_{xt} + u_o \tfrac{\partial h_{xt}}{\partial x} \quad & + u_t \tfrac{\partial h_{xo}}{\partial x} + v_o \tfrac{\partial h_{xt}}{\partial y} + v_t \tfrac{\partial h_{xo}}{\partial y} - h_{xo}\tfrac{\partial u_t}{\partial x} - h_{xt}\tfrac{\partial u_o}{\partial x} - h_{yo}\tfrac{\partial u_t}{\partial y} \\ & - h_{yt}\tfrac{\partial u_o}{\partial y} = \tfrac{1}{\gamma}\tfrac{\partial^2 h_{xt}}{\partial y^2} \end{aligned} \tag{18}$$

$$i\omega\theta_t + u_o\frac{\partial \theta_t}{\partial x} + u_t\frac{\partial \theta_o}{\partial x} + v_o\frac{\partial \theta_t}{\partial y} + v_t\frac{\partial \theta_o}{\partial y} = \frac{1}{P_r}\frac{\partial^2 \theta_t}{\partial y^2} + 2\zeta u_o u_t + 2E_c\left(\frac{\partial u_o}{\partial y}\cdot\frac{\partial u_t}{\partial y}\right) \tag{19}$$

along with boundary conditions:

$$u_t = v_t = 0\ ,\ \theta_t = 1\ ,\ h_{yt} = 0,\ h_{xt} = 1, \text{at } y = 0 \tag{20}$$

$$u_t \to 1,\ \theta_t \to 1,\ h_{xt} \to 0\ ,\ \text{as } y \to \infty$$

Now, introducing the following group of primitive variable formulations for the dependent and independent variables of steady and unsteady parts using Equation (21),

$$\begin{gathered} u_0 = U(X,Y),\ v_0 = X^{-\frac{1}{2}}V(X,Y),\ \theta_0 = \theta(X,Y),\ \mathrm{h}_{x0} = \psi_{xs}(X,Y),\ h_{yo} = x^{\frac{-1}{2}}\psi_{ys}(X,Y), \\ x = X,\ \ y = X^{-\frac{1}{2}}Y \end{gathered} \tag{21}$$

The fluctuating portion is once more transformed into calculations, both imaginary and real. By taking into account [30–34] and utilizing the Stokes coefficients for fluctuations presented in Formula (22), the relationship between both real and imaginary forms may be discovered.

$$u_t = u_1 + iu_2,\ v_t = v_1 + iv_2,\ \theta_t = \theta_1 + i\theta_2,\ \psi_t = \psi_1 + i\psi_2 \tag{22}$$

Primitive Steady Equations:

$$X\frac{\partial U}{\partial X} - \frac{1}{2}Y\frac{\partial U}{\partial Y} + \frac{\partial V}{\partial Y} = 0 \tag{23}$$

$$\begin{gathered} XU_s\tfrac{\partial U_s}{\partial X} + \left[V_s - \tfrac{Y}{2}U_s\right]\tfrac{\partial U_s}{\partial Y} \\ = \tfrac{\partial^2 U_s}{\partial Y^2} + \xi\left[X\psi_{xs}\tfrac{\partial \psi_{xs}}{\partial Y} + \left(\psi_{ys} - \tfrac{Y}{2}\psi_{xs}\right)\tfrac{\partial \psi_{xs}}{\partial Y}\right] + \lambda\theta\ sin\alpha \end{gathered} \tag{24}$$

$$X\frac{\partial \psi_{xs}}{\partial X} - \frac{Y}{2}\frac{\partial \psi x_s}{\partial Y} + \frac{\partial \psi_{ys}}{\partial Y} = 0 \tag{25}$$

$$XU_s\frac{\partial \psi_{xs}}{\partial X} + \left[V_s - \frac{Y}{2}U_s\right]\frac{\partial \psi_{xs}}{\partial Y} - X\psi_{xs}\frac{\partial U_s}{\partial X} - \left(\psi_{ys} - \frac{Y}{2}\psi_{xs}\right)\frac{\partial U_s}{\partial Y} = \frac{1}{\gamma}\frac{\partial^2 \psi_{xs}}{\partial Y^2} \tag{26}$$

$$XU_s\frac{\partial \theta_s}{\partial X} + \left[V_s - \frac{Y}{2}U_s\right]\frac{\partial \theta_s}{\partial Y} = \frac{1}{P_r}\frac{\partial^2 \theta_s}{\partial Y^2} + \zeta {U_s}^2 + E_c\left(\frac{\partial U_s}{\partial Y}\right)^2 \tag{27}$$

$$U = V = 0,\ \theta = 1\ ,\ \psi_{ys} = 0\ ,\ \psi_{xs} = 1, \text{at } Y = 0 \tag{28}$$

$$U \to 1,\ \theta \to 1,\ \psi_{xs} \to 0\ ,\ \text{as}\ Y \to \infty.$$

Primitive Real Equations:

$$X\frac{\partial U_1}{\partial X} - \frac{1}{2}Y\frac{\partial U_1}{\partial Y} + \frac{\partial V_1}{\partial Y} = 0 \tag{29}$$

$$\begin{aligned} X\left[U_s\tfrac{\partial U_1}{\partial X} + U_1\tfrac{\partial U_s}{\partial X}\right] &+ \left[V_s - \tfrac{Y}{2}U_s\right]\tfrac{\partial U_1}{\partial Y} + \left[V_1 - \tfrac{Y}{2}U_1\right]\tfrac{\partial U_s}{\partial Y} - \omega X(U_2 + 1) \\ &= \tfrac{\partial^2 U_1}{\partial Y^2} \\ &+\xi\left[X\left(\psi_{xs}\tfrac{\partial \psi_{x1}}{\partial x} + \psi_{x1}\tfrac{\partial \psi_{xs}}{\partial x}\right) + \left(\psi_{ys} - \tfrac{Y}{2}\psi_{xs}\right)\tfrac{\partial \psi_{x1}}{\partial Y} + \left(\psi_{y1} - \tfrac{Y}{2}\psi_{x1}\right)\tfrac{\partial \psi_{xs}}{\partial Y}\right] \\ &+\lambda\theta sin\alpha \end{aligned} \tag{30}$$

$$X\frac{\partial \psi_{x1}}{\partial X} - \frac{Y}{2}\frac{\partial \psi_{x1}}{\partial Y} + \frac{\partial \psi_{y1}}{\partial Y} = 0 \tag{31}$$

$$\begin{aligned} X\left[U_s\tfrac{\partial \psi x_1}{\partial X} + U_1\tfrac{\partial \psi x_s}{\partial X}\right] &+ \left[V_s - \tfrac{Y}{2}U_s\right]\tfrac{\partial \psi x_1}{\partial Y} + \left[V_1 - \tfrac{Y}{2}U_1\right]\tfrac{\partial \psi x_s}{\partial Y} - \omega X\psi x_2 \\ &-\left[X\left(\psi_{xs}\tfrac{\partial U_1}{\partial x} + \psi_{x1}\tfrac{\partial U_s}{\partial x}\right) + \left(\psi_{ys} - \tfrac{Y}{2}\psi_{xs}\right)\tfrac{\partial U_1}{\partial Y} + \left(\psi_{y1} - \tfrac{Y}{2}\psi_{x1}\right)\tfrac{\partial U_s}{\partial Y}\right] = \tfrac{1}{\gamma}\tfrac{\partial^2 \psi x_1}{\partial Y^2} \end{aligned} \tag{32}$$

$$\begin{aligned} X\left[U_s\tfrac{\partial \theta_1}{\partial X} + U_1\tfrac{\partial \theta_s}{\partial X}\right] + \left[V_s - \tfrac{Y}{2}U_s\right]\tfrac{\partial \theta_1}{\partial Y} + \left[V_1 - \tfrac{Y}{2}U_1\right]\tfrac{\partial \theta_s}{\partial Y} - \omega X\theta_2 \\ = \tfrac{1}{P_r}\tfrac{\partial^2 \theta_1}{\partial Y^2} + 2\zeta U_s U_1 + 2E_c\left(\tfrac{\partial U_s}{\partial Y}\cdot\tfrac{\partial U_1}{\partial Y}\right) \end{aligned} \tag{33}$$

$$U_1 = V_1 = 0\ ,\ \theta_1 = 1\ ,\ \psi_{y1} = 0,\ \psi_{x1} = 1\ \text{at}\ Y = 0 \tag{34}$$

$$U_1 \to 1,\ \theta_1 \to 0\ ,\ \psi_{x1} \to 0\ ,\ \text{as}\ Y \to \infty$$

Primitive Imaginary Equations:

$$X\frac{\partial U_2}{\partial X} - \frac{1}{2}Y\frac{\partial U_2}{\partial Y} + \frac{\partial V_2}{\partial Y} = 0 \tag{35}$$

$$\begin{aligned} X\left[U_s\tfrac{\partial U_2}{\partial X} + U_2\tfrac{\partial U_s}{\partial X}\right] &+ \left[V_s - \tfrac{Y}{2}U_s\right]\tfrac{\partial U_2}{\partial Y} + \left[V_2 - \tfrac{Y}{2}U_2\right]\tfrac{\partial U_s}{\partial Y} + \omega X(U_1 - 1) \\ &= \tfrac{\partial^2 U_2}{\partial Y^2} \\ &+\xi\left[X\left(\psi_{xs}\tfrac{\partial \psi_{x2}}{\partial x} + \psi_{x2}\tfrac{\partial \psi_{xs}}{\partial x}\right) + \left(\psi_{ys} - \tfrac{Y}{2}\psi_{xs}\right)\tfrac{\partial \psi_{x2}}{\partial Y} + \left(\psi_{y2} - \tfrac{Y}{2}\psi_{x2}\right)\tfrac{\partial \psi_{xs}}{\partial Y}\right] \\ &+\lambda\theta sin\alpha \end{aligned} \tag{36}$$

$$X\frac{\partial \psi_{x1}}{\partial X} - \frac{Y}{2}\frac{\partial \psi_{x1}}{\partial Y} + \frac{\partial \psi_{y1}}{\partial Y} = 0 \tag{37}$$

$$\begin{aligned} X\left[U_s\tfrac{\partial \psi_{x2}}{\partial X} + U_2\tfrac{\partial \psi x_s}{\partial X}\right] &+ \left[V_s - \tfrac{Y}{2}U_s\right]\tfrac{\partial \psi x_2}{\partial Y} + \left[V_2 - \tfrac{Y}{2}U_2\right]\tfrac{\partial \psi x_s}{\partial Y} + \omega X\varphi_1 \\ &-\left[X\left(\psi_{xs}\tfrac{\partial U_2}{\partial x} + \psi_{x2}\tfrac{\partial U_s}{\partial x}\right) + \left(\psi_{ys} - \tfrac{Y}{2}\psi_{xs}\right)\tfrac{\partial U_2}{\partial Y} + \left(\psi_{y2} - \tfrac{Y}{2}\psi_{x2}\right)\tfrac{\partial U_s}{\partial Y}\right] \\ &= \tfrac{1}{\gamma}\tfrac{\partial^2 \psi_2}{\partial Y^2} \end{aligned} \tag{38}$$

$$\begin{aligned} X\left[U_s\tfrac{\partial \theta_2}{\partial X} + U_2\tfrac{\partial \theta_s}{\partial X}\right] + \left[V_s - \tfrac{Y}{2}U_s\right]\tfrac{\partial \theta_2}{\partial Y} + \left[V_2 - \tfrac{Y}{2}U_2\right]\tfrac{\partial \theta_s}{\partial Y} + \omega X\theta_1 \\ = \tfrac{1}{P_r}\tfrac{\partial^2 \theta_2}{\partial Y^2} + 2\zeta U_s U_2 + 2E_c\left(\tfrac{\partial U_s}{\partial Y}\cdot\tfrac{\partial U_2}{\partial Y}\right) \end{aligned} \tag{39}$$

$$U_2 = V_2 = 0,\ \theta_2 = 0,\ \psi_{y2} = 0,\ \psi_{x2} = 0,\ \text{at}\ Y = 0 \tag{40}$$

$$U_2 \to 0,\ \theta_2 \to 0,\ \psi_{x2} \to 0\ ,\ \text{as}\ Y \to \infty.$$

3. Computing Technique

The primitive formed steady, real and imaginary models are evaluated with the help of an implicit finite difference scheme. The systems of obtained algebraic equations are solved numerically by using the Gaussian elimination approach in terms of a global matrix. The matrix-formed expressions are explored graphically and statistically via programming tool FORTRAN and Tecplot-360. The oscillatory profiles of steady, real and imaginary components with unknown quantities U, V, θ and φ are illustrated by Formula (41), where, A_s, A_t and A_m are amplitudes and α_s, α_t and α_m are phase angles. The geometrical results of periodical shear stress τ_s, magnetic flux τ_m, and heat transfer τ_t along the horizontal cylinder are evaluated at prominent inclined positions.

$$\begin{aligned} \tau_s &= \left(\frac{\partial U}{\partial Y}\right)_{y=0} + \varepsilon|A_s|Cos(\omega t + \alpha_s), \\ \tau_t &= \left(\frac{\partial \theta}{\partial Y}\right)_{y=0} + \varepsilon|A_t|Cos(\omega t + \alpha_t), \\ \tau_m &= \left(\frac{\partial \psi}{\partial Y}\right)_{y=0} + \varepsilon|A_m|Cos(\omega t + \alpha_m), \end{aligned} \tag{41}$$

where,

$$\begin{aligned} &A_s = \left({u_1}^2 + {u_2}^2\right)^{\frac{1}{2}}, \quad A_t = \left({\theta_1}^2 + {\theta_2}^2\right)^{\frac{1}{2}}, \quad A_m = \left({\varphi_{x1}}^2 + {\varphi_{x2}}^2\right)^{\frac{1}{2}}, \\ &\alpha_s = \tan^{-1}(u_2/u_1), \quad \alpha_t = \tan^{-1}(\theta_2/\theta_1), \quad \alpha_m = \tan^{-1}(\varphi_{x2}/\varphi_{x1}). \end{aligned}$$

4. Results and Discussion

In the current research, a changeable mixed convection oscillatory flow of magnetic flux and heat transmission around a magneto-driven cylinder under feasible angles $\pi/3$, $\pi/6$ and π with combined effects of MHD, viscous dissipation and Joule heating effects was numerically simulated. The graphical and numerical findings were explored under convective thermal conditions. The governing computational mechanism was implemented for oscillation and transient characteristics of magnetic flux and friction. A fluctuating dynamic computational framework was suggested for associated forms of partial differential equations under thermo-boundary variables. To make the non-dimensional representation easier to work with for efficient statistical calculations, it was reduced further. Later, for a variety of variables, significant computations were performed via the implicit finite difference methodology.

4.1. Non-Oscillating/Steady Plots of Velocity U, Temperature θ, Magnetic ϕ Region

In Figure 2a, the velocity U increases as the Eckert coefficient E_c increases at angle π with significant amplitude. The temperature θ and magnetic field ϕ are enhanced at angle $\pi/6$ as the Eckert coefficient E_c increases in Figure 2b,c. The minimum difference in each temperature θ and magnetic field ϕ graph is illustrated at both angles. The identical effects of Eckert coefficient E_c is investigated in both θ and ϕ. The influence of Joule heat ζ on velocity U, temperature θ and magnetic ϕ profiles is investigated for $\mathrm{Pr} = 7.0$ under maximum convective forces in Figure 3a,c. The impact of ζ is prominent as U changes from angle $\pi/6$ to π. The θ and ϕ profiles increase for $\zeta = 0.1$ to $\zeta = 0.5$ and gradually decrease for higher values of ζ under dissipative flow. The minimum difference in both θ and ϕ is drafted then U under maximum Joule heat ζ. The increasing behavior of U is confirmed for each Joule heating ζ coefficient under dissipative fluid. It was valid because the Joule heat coefficient ζ acts like a thermal element to improve heat transmission across the magnetic surface. The effects of mixed convection factor λ on velocity U, temperature θ and magnetic ϕ profiles are scrutinized at two angles, $\pi/6$ and π, across the heated cylinder immersed in dissipated fluid in Figure 4a,c. The velocity U distributions improve as buoyancy factor λ grows through both angles. The same increasing effects of both θ and ϕ are noted for minimum $\lambda = 0.1$ at each angle under Joule heat ζ and dissipations E_c. It is expected due to increasing pressure forces that enhance the motion of dissipative fluid around the heated cylinder. Both temperature θ and magnetic field ϕ decline as λ increases at both angles. The important angle for significant results is $\pi/6$ for each parameter. The minimum velocity U behavior is depicted at both angles for each coefficient λ under Joule heating ζ. A notable difference in each plot is gained for every mixed convection coefficient λ. In Figure 5a,c, the implication of Prandtl coefficient Pr for each unknown variable U, θ and ϕ is sketched at two suitable angles, $\pi/6$ and π, under Joule heat ζ and viscosity dissipations E_c. The velocity U increases as Pr decreases due to low viscous fluid at both angles. The lower velocity U behavior is noted for maximum Pr due to higher thickness of dissipative fluid at each angle, $\pi/6$ and π. The temperature θ improves as Pr declines with favorable differences in each line. Moreover, similar characteristics of magnetic field ϕ are examined as Pr increases at both $\pi/6$ and π angles under MHD effects. All results are accurate by matching the given boundaries.

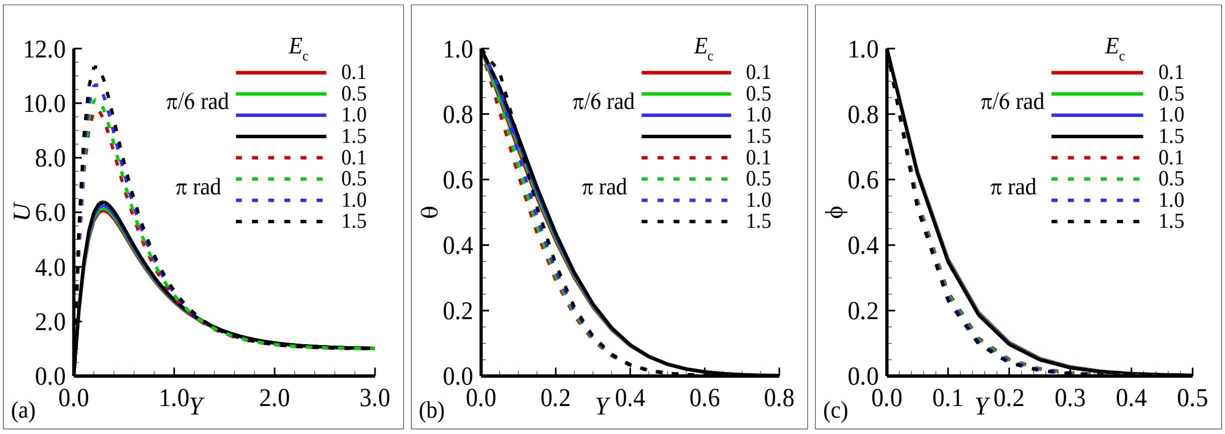

Figure 2. (**a**–**c**) Non-oscillating/steady plots of velocity profile U, temperature distribution θ, and magnetic-field profile ϕ against E_c.

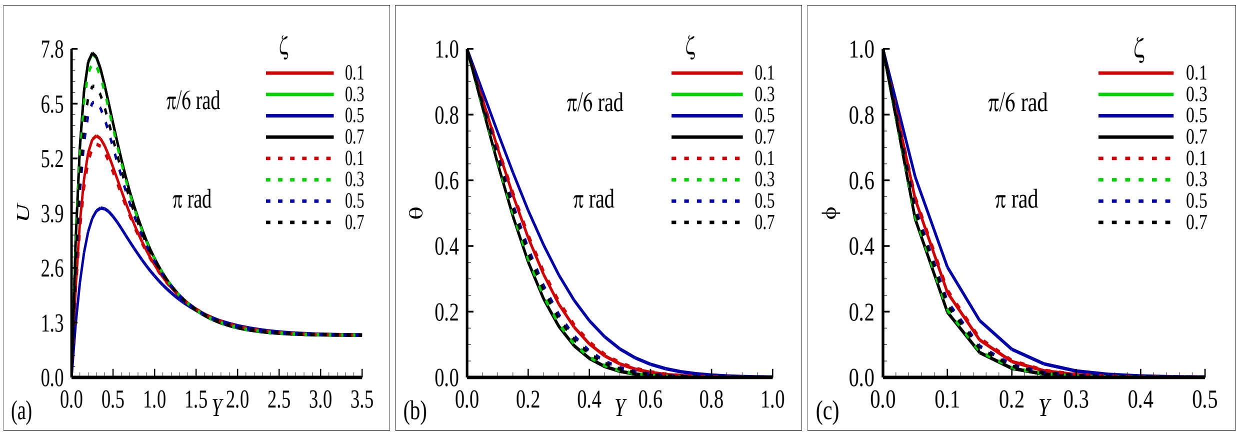

Figure 3. (**a**–**c**) Non-oscillating/steady plots of velocity profile U, temperature distribution θ, and magnetic-field profile ϕ against ζ.

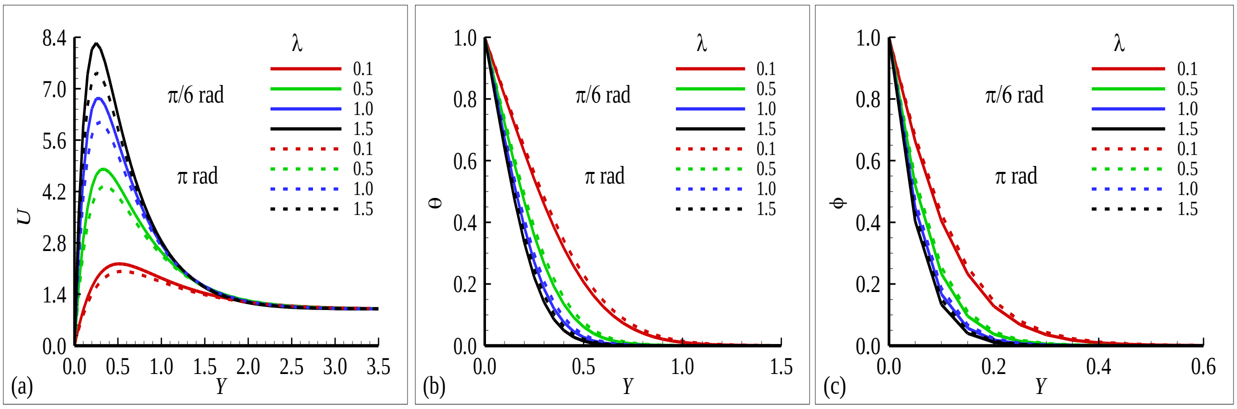

Figure 4. (**a**–**c**) Non-oscillating/steady plots of velocity profile U, temperature distribution θ, and magnetic-field profile ϕ against λ.

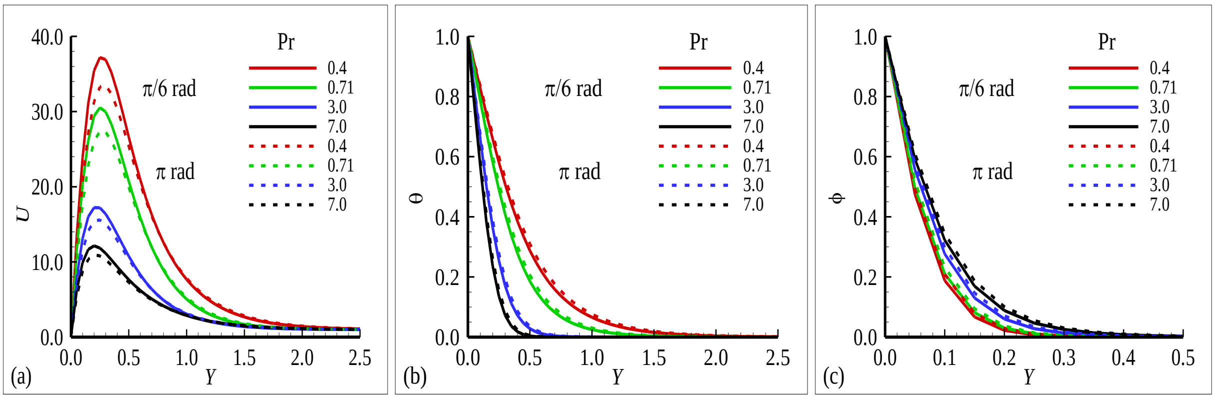

Figure 5. (**a**–**c**) Non-oscillating/steady plots of velocity profile U, temperature distribution θ, and magnetic-field profile ϕ against Pr.

4.2. Oscillatory Representations of Transient Shearing Stress τ_s, Heat Rate τ_t, Magnetic Flux τ_m

The transient and oscillating behavior of shearing stress τ_s, heat rate τ_t and rate of magnetic flux τ_m for several coefficients of Eckert number E_c across three angles, $\pi/6$, $\pi/3$ and π, of a circular cylinder were studied. In Figure 6a, the small frequency in shearing stress τ_s is found for each $E_c = 0.1,\ 0.5$ at all angles. The maximum oscillations in heat transfer τ_t increase as E_c increases at each angle in Figure 6b. The significant fluctuations in magnetic flux improve as E_c grows from angle $\pi/6$ to π under Joule heat in Figure 6c. The most interesting angle for maximum results is $\pi/6$ in each diagram. In Figure 7a, the larger fluctuations in τ_s with the best difference in each line are noted for Joule heat ζ under dissipative flow. The minimum increment in τ_s is obtained for E_c at angle π. In Figure 7b, the intensity of fluctuations in τ_t increases as E_c grows at each angle under viscous dissipations and buoyant forces. It is seen that the oscillations in each graph are enhanced under convective forces. Joule heat increases the heat transport at each angle across the heated cylinder. In Figure 7c, the identical pattern of magnetic flux τ_m is examined at each angle due to dissipation. This was expected because the magnetic surface absorbed the excessive heat due to electrical conducting fluid. In Figure 8a, the small oscillations in shearing stress τ_s are investigated at lower magnetic Prandtl γ, but large oscillations in τ_s are illustrated at higher magnetic Prandtl γ for each angle. The lower difference in τ_t with significant frequency is examined for each γ under Joule heat and dissipations in Figure 8b, since the heat transmission decreases as magnetic Prandtl γ increases to absorb the increasing heat rate. In Figure 8c, the magnetic flux improves as γ grows from angle $\pi/6$ to π across the heated cylinder. The oscillations in magnetic flux decline as γ diminishes at each angle. It is seen that the magnetic flux enhances as magnetic

Prandtl γ increases along each angle. In Figure 9a, the influence of Prandtl coefficient Pr on shearing stress τ_s, heat transmission and magnetic flux is sketched at three significant angles under Joule heat and dissipations. The maximum oscillations in τ_s are enhanced as Pr grows at each angle, with noticeable differences in each line. In Figure 9b, the heat rate decreases as Pr decreases under Joule heat and dissipation from angle $\pi/6$ to π across the heated cylinder. The maximum rate of heat transport is drafted as Pr grows across each angle of the stationary cylinder. In Figure 9c, a similar trend in magnetic flux is sketched for each Pr under maximum Joule heat and dissipations, since maximum magnetic field decreases the heat transmission across each position of the stationary cylinder.

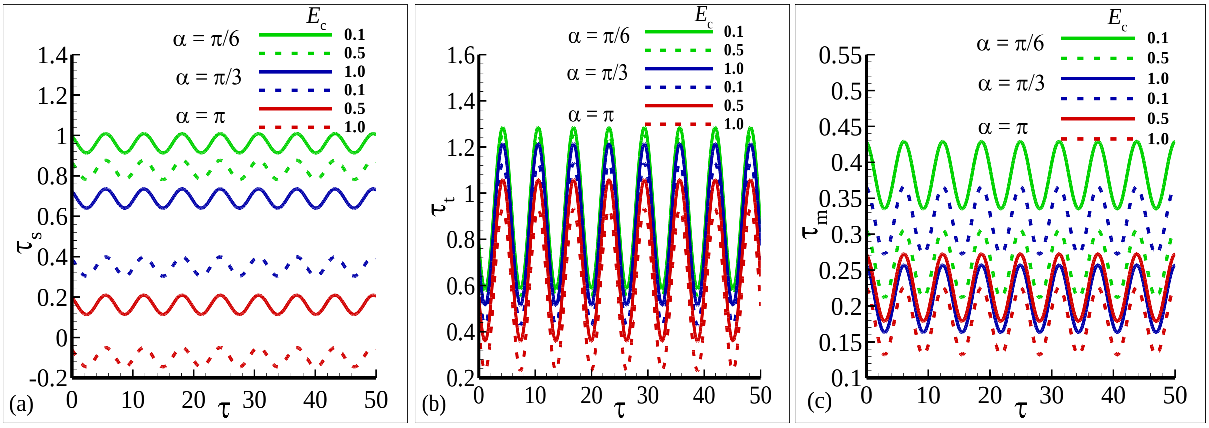

Figure 6. (**a**–**c**) The oscillatory representations of τ_s, τ_m, τ_t against E_c.

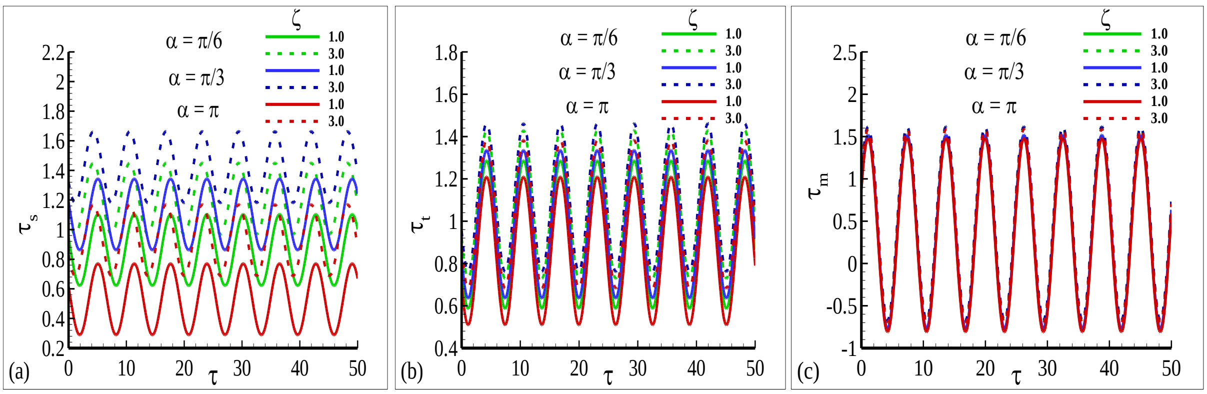

Figure 7. (**a**–**c**) The oscillatory representations of τ_s, τ_m, τ_t against ζ.

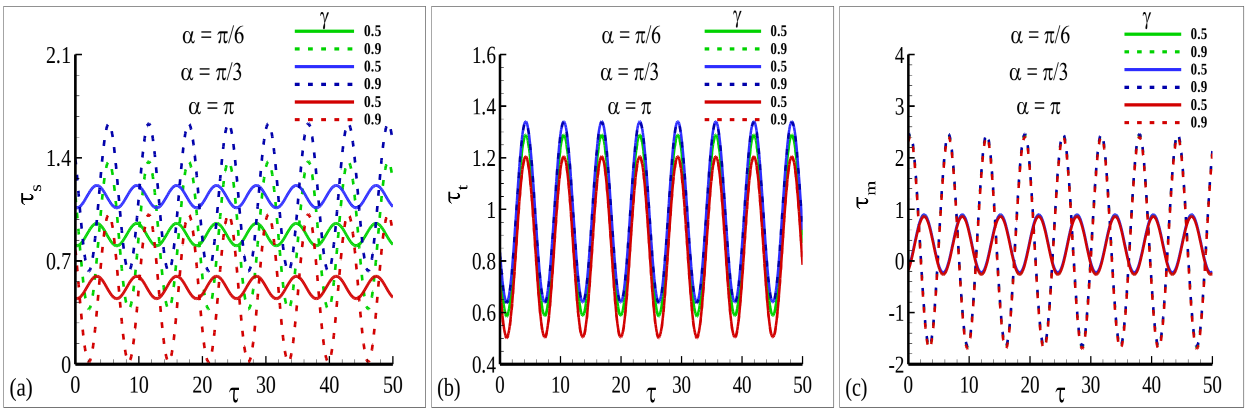

Figure 8. (**a**–**c**) The oscillatory representations of τ_s, τ_m, τ_t against γ.

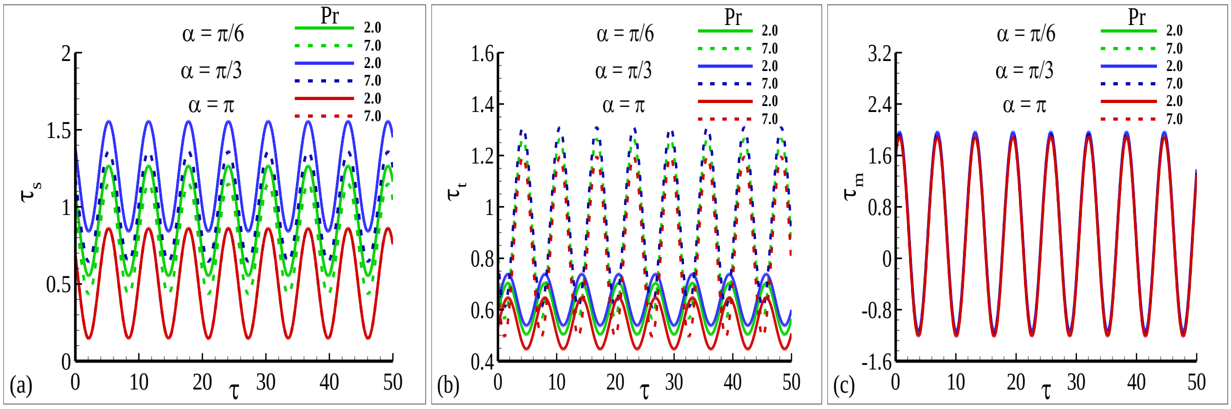

Figure 9. (**a–c**) The oscillatory representations of τ_s, τ_m, τ_t against Pr.

Table 1 compares the calculated shearing stress τ_s results with previously published research by Chawla [35] using multiple attractive magnetic Prandtl γ factor options based on the effect of a vertically applied magnetic field throughout a warmed and magnetized cylinder. The significant shearing stress τ_s is achieved by electromagnetic influences for every γ. Furthermore, the present shearing stress τ_s outcomes are consistent with previously reported findings. Table 2 demonstrates that the magnitude of heat transmission is minimal near angle $\alpha = 1.4$ but maximal near $\alpha = 0.0$ and π according to different electromagnetic Prandtl coefficient values. The significant position for the transmission of heat may be found in the range of $\alpha = 0.0,\ \pi$ with different ranges of $\gamma = 0.2,\ 0.4,\ 0.8$ and 1.5. The growing characteristic of heat transmission is shown from $\alpha = 1.4$ to $\alpha = \pi$, and then decreases from $\alpha = 0.0$ to $\alpha = 1.4$. The lowest value of heat rate is noted at $\alpha = 1.4$ across the magnetic cylinder.

Table 1. Numerical findings of skin friction around magnetized and heated cylinder under feasible values of magneto Prandtl parameter $\gamma = 1.0,\ 10.0$ and 100.0.

γ	Chawla [35]	Present Results	Percentage Error
1	0.3204	0.3210	0.1872%
10	0.3210	0.3207	0.0934%
100	0.3244	0.3196	1.4796%

Table 2. Four distinct choices of γ = 0.2, 0.4, 0.8, 1.5 for numerical findings of heat transfer τ_t along various angles α of magnetized cylinder.

α	γ = 0.2	γ = 0.4	γ = 0.8	γ = 1.5
0.0	0.1632	0.1514	0.1431	0.1397
0.2	0.1128	0.1367	0.1243	0.1156
0.4	0.0956	0.1013	0.1017	0.1073
0.6	0.0890	0.0987	0.0987	0.1011
0.8	0.0853	0.0913	0.0951	0.0989
1.0	0.0821	0.0885	0.0909	0.0933
1.2	0.0834	0.0831	0.0875	0.0880
1.4	0.0786	0.0792	0.0710	0.0871
1.6	0.0791	0.0835	0.0797	0.0913
1.8	0.0798	0.0857	0.0841	0.0957
2.0	0.0814	0.0891	0.0879	0.0993
2.2	0.0824	0.0919	0.0911	0.1015
2.4	0.0873	0.0995	0.0959	0.1037
2.6	0.0889	0.1031	0.1020	0.1071

Table 2. *Cont.*

α	γ = 0.2	γ = 0.4	γ = 0.8	γ = 1.5
2.8	0.1145	0.1169	0.1095	0.1131
3.0	0.1170	0.1187	0.1131	0.1179
π	0.1627	0.1439	0.1413	0.1337

5. Conclusions

To insulate increasing heat rate, the aligned magnetic characteristics across circular geometries are very important in engineering and advanced technological devices. The magnetized devices contribute a significant impact in microchips to reduce cracking and overheating. In the current research, changeable mixed convection oscillatory flow of magnetic flux and heat transmission around a magneto-driven cylinder under feasible angles $\pi/3$, $\pi/6$ and π with combined effects of MHD, viscous dissipation and Joule heating effects was numerically simulated. The graphical and numerical findings were explored under convective thermal conditions. The governing computational mechanism was applied for oscillation and transient characteristics of magnetic flux and friction. A fluctuating dynamic computational framework was suggested for associated forms of partial differential equations under thermo-boundary variables. The complex equations were converted into a non-dimensional format by using the necessary non-dimensional components. To make the non-dimensional representation easier to work with for efficient statistical calculations, it was reduced further. The present thermal and electromagnetic hydrodynamics mechanism is important for nanoburning and magneto-resonance scanning approaches. The computational and tabular results for different growing elements via attractive options were obtained. The significant key points are addressed below.

- The prominent amplitude quantity of the velocity U was examined at $\zeta = 3.0$ across angle $\pi/3$, but enhanced results of Joule heating ζ for the temperature θ plot were deduced at angle $\pi/6$.
- Prominent improvement in temperature θ was investigated at angles $\pi/3$, $\pi/6$ and π with the Joule heating impacts. The result was theoretically possible since viscous dissipation and Joule heating have been employed as source inputs for assessing the transfer efficiency of heat in magnetically conducting fluids.
- Since the force of buoyancy works like an external pressure component to increase fluid speed, the enhanced Pr through viscous dissipation and Joule heating led to the noticeable augmentation in electromagnetic diagrams.
- The higher amplitude of oscillation in τ_t at each circular position was evaluated under viscous dissipation and Joule heating at angle $\pi/3$. This was technically predicted since the frequency of fluid movement rises due to gravitational pull, which improves the intensity of the oscillating heat and oscillating magnetic flux of water-based fluids.
- Assuming the significance of the three angles $\pi/3$, $\pi/6$ and π, the minimal magnitude of oscillation in a magnetic flux was investigated due to viscous dissipation and Joule heating.
- The magnitude of fluctuating heat transfer τ_t was improved under maximum Pr at every location $\pi/3$, $\pi/6$ and π compared to other plots. For each Pr option around the entire magnetized cylinder, the same behavior in a magnetic flux with suitable magnitude was developed.

Author Contributions: Conceptualization, Z.U., M.S.A. and M.A.Q.; Methodology, Z.U.; Software, Z.U., M.S.A. and M.A.Q.; Validation, Z.U., M.S.A. and M.A.Q.; Formal analysis, M.S.A.; Investigation, M.S.A. and M.A.Q.; Resources, M.A.Q.; Data curation, M.A.Q.; Writing—original draft, Z.U.; Supervision, Z.U. All authors have read and agreed to the published version of the manuscript.

Funding: This research received no external funding.

Data Availability Statement: Data sharing is not applicable to this article.

Conflicts of Interest: The authors declare no conflict of interest.

Nomenclature

u, v, U	Velocity along x and y-direction (m s^{-1})
H_x, H_y, ϕ	Magnetic velocities along x and y directions (Tesla)
μ	Dynamic viscosity (kg m^{-1} s^{-1})
ν	Kinematic viscosity (m^2 s^{-1})
ρ	Fluid density (kg m^{-3})
g	Gravitational acceleration (m s^{-2})
β	Thermal expansion coefficient (K^{-1})
ν_m	Magnetic permeability (H m^{-1})
α	Thermal diffusivity (m^2 s^{-1})
T	Temperature (K)
C_p	Specific heat (J kg^{-1} K^{-1})
σ	Electrical conductivity (s m^{-1})
T_∞	Ambient temperature (K)
R_{e_L}	Reynolds number
G_{r_L}	Grashof number
ζ	Joule heating parameter
τ	Shearing stress (Pa)
ξ	Magnetic force parameter
λ	Mixed convection parameter
θ	Dimensionless temperature
γ	Magnetic Prandtl number
Pr	Prandtl number
E_c	Eckert number
ΔT	Temperature difference

References

1. Poornima, T.; Sreenivasulu, P.; Bhaskar Reddy, N. Chemical reaction effects on an unsteady MHD mixed convective and radiative boundary layer flow over a circular cylinder. *J. Appl. Fluid Mech.* **2016**, *9*, 2877–2885. [CrossRef]
2. Shafie, S.; Mahat, R.; Januddi, F. Numerical Solutions of Mixed Convection Flow Past a Horizontal Circular Cylinder with Viscous Dissipation in Viscoelastic Nanofluid. *J. Adv. Res. Micro Nano Eng.* **2020**, *1*, 24–37.
3. Mohamed, M.K.A.; Sarif, N.M.; Noar, N.A.Z.M.; Salleh, M.Z.; Ishak, A.M. Mixed convection boundary layer flow on a horizontal circular cylinder in a nanofluid with viscous dissipation effect. *Malays. J. Fundam. Appl. Sci.* **2018**, *14*, 32–39.
4. Anwar, I.; Amin, N.; Pop, I. Mixed convection boundary layer flow of a viscoelastic fluid over a horizontal circular cylinder. *Int. J. Non-Linear Mech.* **2008**, *43*, 814–821. [CrossRef]
5. Aboud, E.D.; Rashid, H.K.; Jassim, H.M.; Ahmed, S.Y.; Khafaji, S.O.W.; Hamzah, H.K.; Ali, F.H. MHD effect on mixed convection of annulus circular enclosure filled with Non-Newtonian nanofluid. *Heliyon* **2020**, *6*, e03773. [CrossRef] [PubMed]
6. Ismail, M.A.; Mohamad, N.F.; Ilias, M.R.; Shafie, S. MHD Effect on Unsteady Mixed Convection Boundary Layer Flow past a Circular Cylinder with Constant Wall Temperature. *J. Phys. Conf. Ser.* **2017**, *890*, 012054. [CrossRef]
7. Makanda, G.; Shaw, S.; Sibanda, P. Effects of radiation on MHD free convection of a Casson fluid from a horizontal circular cylinder with partial slip in non-Darcy porous medium with viscous dissipation. *Bound. Value Probl.* **2015**, *2015*, 75. [CrossRef]
8. Gireesha, B.J.; Mahanthesh, B.; Gorla, R.S.R.; Krupalakshmi, K.L. Mixed convection two-phase flow of Maxwell fluid under the influence of non-linear thermal radiation, non-uniform heat source/sink and fluid-particle suspension. *Ain Shams Eng. J.* **2018**, *9*, 735–746. [CrossRef]
9. Al-Farhany, K.; Al-Muhja, B.; Loganathan, K.; Periyasamy, U.; Ali, F.; Sarris, I.E. Analysis of Convection Phenomenon in Enclosure Utilizing Nanofluids with Baffle Effects. *Energies* **2022**, *15*, 6615. [CrossRef]
10. Al-Mdallal, Q.; Prasad, V.R.; Basha, H.T.; Sarris, I.; Akkurt, N. Keller box simulation of magnetic pseudoplastic nano-polymer coating flow over a circular cylinder with entropy optimisation. *Comput. Math. Appl.* **2022**, *118*, 132–158. [CrossRef]
11. Zhang, X.F.; Yang, J.C.; Ni, M.J.; Zhang, N.M.; Yu, X.G. Numerical simulations of flow around dual tandem circular cylinders under a strong axial magnetic field. *Phys. Fluids* **2023**, *35*, 023604. [CrossRef]
12. Naghshineh, N.; Barlow, N.S.; Samaha, M.A.; Weinstein, S.J. Asymptotically consistent analytical solutions for the non-Newtonian Sakiadis boundary layer. *Phys. Fluids* **2023**, *35*, 053103. [CrossRef]
13. Khan, A.S.; Xu, H.Y.; Nie, Y.; Idrees, M.; Khan, N.U.S. Numerical examination of wall properties for the magnetohydrodynamics stagnation point flow of micro-rotating fluid subject to weak concentration. *Phys. Fluids* **2023**, *35*, 053102. [CrossRef]

14. Wu, X.; Liu, C.; Bai, Y.; Zhang, Y.; Pan, M.; Wang, X. Magnetic diffusion of time distributed-order Maxwell fluid in boundary layer under the action of induced magnetic field. *Phys. Fluids* **2023**, *35*, 053108.
15. Hayat, T.; Shaheen, U.; Shafiq, A.; Alsaedi, A.; Asghar, S. Marangoni mixed convection flow with Joule heating and nonlinear radiation. *AIP Adv.* **2015**, *5*, 077140. [CrossRef]
16. Maurya, P.K.; Deo, S.; Maurya, D.K. Couple stress fluid flow enclosing a solid sphere in a porous medium: Effect of magnetic field. *Phys. Fluids* **2023**, *35*, 072006. [CrossRef]
17. Routa, C.; Balaji, P.; Sahu, A.K. Numerical investigation of effect of surface pattern and rotation on power-law fluid flow and heat transfer around a cylinder in laminar flow regime. *Phys. Fluids* **2023**, *35*, 073101. [CrossRef]
18. Lv, J.; Zhang, Y. Numerical study of the natural transition of water boundary layers over heated/cooled flat plates. *Phys. Fluids* **2023**, *35*, 064106.
19. Ankush, A.; Narayana, P.A.L.; Sahu, K.C. Mixed convection instability in a viscosity stratified flow in a vertical channel. *Phys. Fluids* **2023**, *35*, 064114. [CrossRef]
20. Govindarajulu, K.; Subramanyam Reddy, A. Magnetohydrodynamic pulsatile flow of third grade hybrid nanofluid in a porous channel with Ohmic heating and thermal radiation effects. *Phys. Fluids* **2022**, *34*, 013105. [CrossRef]
21. Ilin, K.; Morgulis, A. The effect of boundary conditions on the stability of two-dimensional flows in an annulus with permeable boundary. *Phys. Fluids* **2022**, *34*, 074117. [CrossRef]
22. Kumar, G.C.; Reddy, K.J.; Konijeti, R.K.; Reddy, M.N. Non-uniform heat source/sink and joule heating effects on chemically radiative MHD mixed convective flow of micropolar fluid over a stretching sheet in porous medium. In *Defect and Diffusion Forum*; Trans Tech Publications Ltd.: Bäch, Switzerland, 2018; Volume 388, pp. 281–302.
23. Kumar, P.V.; Ibrahim, S.M.; Lorenzini, G. Impact of thermal radiation and Joule heating on MHD mixed convection flow of a Jeffrey fluid over a stretching sheet using homotopy analysis method. *Int. J. Heat Technol.* **2017**, *35*, 978–986. [CrossRef]
24. Roy, N.C.; Akther, P.; Halder, A.K. MHD mixed convection flow of a micropolar fluid past a wedge fixed in a fluctuating free stream and surface temperature. *Dhaka Univ. J. Sci.* **2016**, *64*, 65–70. [CrossRef]
25. Roy, N.C.; Hossain, M.A. Unsteady laminar mixed convection boundary layer flow near a vertical wedge due to oscilations in the free-stream and surface temperature. *Int. J. Appl. Mech. Eng.* **2016**, *21*, 169–186. [CrossRef]
26. Firoza, M.N.; Roy, N.C.; Hossain, M.A. Conjugate heat and mass transfer on fluctuating mixed convection flow along a vertical wedge with thermal radiation. *Int. J. Appl. Mech. Eng.* **2017**, *22*, 539–565. [CrossRef]
27. Hossain, M.A.; Roy, N.C.; Siddiqa, S. Unsteady mixed convection dusty fluid flow past a vertical wedge due to small fluctuation in free stream and surface temperature. *Appl. Math. Comput.* **2017**, *293*, 480–492. [CrossRef]
28. Maranna, T.; Sneha, K.N.; Mahabaleshwar, U.S.; Sarris, I.E.; Karakasidis, T.E. An Effect of Radiation and MHD Newtonian Fluid over a Stretching/Shrinking Sheet with CNTs and Mass Transpiration. *Appl. Sci.* **2022**, *12*, 5466. [CrossRef]
29. Mabood, F.; Fatunmbi, E.O.; Benos, L.; Sarris, I.E. Entropy Generation in the Magnetohydrodynamic Jeffrey Nanofluid Flow over a Stretching Sheet with Wide Range of Engineering Application Parameters. *Int. J. Appl. Comput. Math.* **2022**, *8*, 98. [CrossRef]
30. Alharbi, K.A.M.; Ullah, Z.; Jabeen, N.; Ashraf, M. Magnetohydrodynamic and Thermal Performance of Electrically Conducting Fluid along the Symmetrical and Vertical Magnetic Plate with Thermal Slip and Velocity Slip Effects. *Symmetry* **2023**, *15*, 1148. [CrossRef]
31. Ullah, Z.; Ahmad, H.; Khan, A.A.; Aldhabani, M.S.; Alsulami, S.H. Thermal conductivity effects on mixed convection flow of electrically conducting fluid along vertical magnetized plate embedded in porous medium with convective boundary condition. *Mater. Today Commun.* **2023**, *35*, 105892. [CrossRef]
32. Ullah, Z.; Jabeen, N.; Khan, M.U. Amplitude and Phase Angle of Oscillatory Heat Transfer and Current Density along a Nonconducting Cylinder with Reduced Gravity and Thermal Stratification Effects. *Mathematics* **2023**, *11*, 2134. [CrossRef]
33. Khan, M.N.; Ullah, Z.; Wang, Z.; Gamaoun, F.; Eldin, S.M.; Ahmad, H. Analysis of fluctuating heat and current density of mixed convection flow with viscosity and thermal conductivity effects along horizontal nonconducting cylinder. *Case Stud. Therm. Eng.* **2023**, *46*, 103023. [CrossRef]
34. Ullah, Z.; Ehsan, M.; Ahmad, H.; Ilyas, A. Combined effects of MHD and slip velocity on oscillatory mixed convective flow around a non-conducting circular cylinder embedded in a porous medium. *Case Stud. Therm. Eng.* **2022**, *38*, 102341. [CrossRef]
35. Chawla, S.S. Magnetohydrodynamic oscillatory flow past a semi-infinite flat plate. *Int. J. Non-Linear Mech.* **1971**, *6*, 117–134. [CrossRef]
36. Dai, B.; Qi, H.; Liu, S.; Zhong, Z.; Li, H.; Song, M.; Ma, M.; Sun, Z. Environmental and economical analyses of transcritical CO_2 heat pump combined with direct dedicated mechanical subcooling (DMS) for space heating in China. *Energy Convers. Manag.* **2019**, *198*, 111317. [CrossRef]
37. Dai, B.; Wang, Q.; Liu, S.; Wang, D.; Yu, L.; Li, X.; Wang, Y. Novel configuration of dual-temperature condensation and dual-temperature evaporation high-temperature heat pump system: Carbon footprint, energy consumption, and financial assessment. *Energy Convers. Manag.* **2023**, *292*, 117360. [CrossRef]